



**Engineering  
and Technology**

### Keywords

Baldwin and Lomax Model,  
Wilcox Model,  
Menter and Rumsey Model,  
Kergaravat and Knight Model,  
Reynolds Averaged  
Navier-Stokes Equations,  
Algebraic and Two-Equation  
Turbulence Models

Received: June 7, 2015

Revised: June 16, 2015

Accepted: June 17, 2015

# Assessment of Several Turbulence Models as Applied to Supersonic Flows in 2D – The Final Choice

Edisson S. G. Maciel

Aeronautical Engineering Division (IEA), Aeronautical Technological Institute (ITA), SP, Brasil

### Email address

[edisavio@edissonsavio.eng.br](mailto:edisavio@edissonsavio.eng.br)

### Citation

Edisson S. G. Maciel. Assessment of Several Turbulence Models as Applied to Supersonic Flows in 2D – The Final Choice. *Engineering and Technology*. Vol. 2, No. 5, 2015, pp. 276-283.

### Abstract

In the present work, the Van Leer flux vector splitting scheme is implemented to solve the two-dimensional Favre-averaged Navier-Stokes equations. The Baldwin and Lomax, Wilcox, Menter and Rumsey, and Kergaravat and Knight turbulence models are used in order to close the problem. The physical problem under study is the supersonic flow along a ramp. The results have demonstrated that the Kergaravat and Knight model in its Launder and Spalding variant captured the boundary layer detachment with consequent detection of circulation bubble formation. The shock angle is better predicted by the Kergaravat and Knight model in its Launder and Spalding variant.

## 1. Introduction

The present work consisted in an evaluation of seventeen turbulence models applied to aerospace problems in the supersonic flow regime. This work was divided in four parts: [1-4], each one composed of four turbulence models, being the last, [4], composed of five turbulence models. The Favre-Averaged Navier-Stokes equations, in a conservative and integral form, were structured discretized and solved explicitly by the [5] algorithm, which performed the numerical experiments. The spatially variable time step was employed to accelerate the convergence of both fluid dynamic and turbulence fields. This tool has presented excellent performance in accelerating the convergence of numerical schemes, as reported in [6-7]. All turbulence models were algebraic, one-equation, or two-equation ones, being  $k-\epsilon$  or  $k-\omega$  variants.

The first paper of this work, [1], has studied the [8-11] turbulence models, applied to the problem of the supersonic flow along a simplified version of the VLS (Brazilian “Satellite Launcher Vehicle”). The [8] and [11] were algebraic models and [9-10] were two-equation models. Excellent results were obtained by the [11] model, highlighting this one as the best choice to this group of options. The excellent capture of the normal shock ahead of the configuration and excellent estimative of the stagnation pressure at the blunt body nose pointed out this turbulence model as the best.

The second paper, [2], left with the [12-15] turbulence models, applied to the same problem aforementioned. The [15] model was algebraic and the others were two-equation models. The [14] turbulence model has provided the second best estimative of the lift aerodynamic coefficient and the best estimative of the stagnation pressure, resulting in its choice as the best of this group of turbulence models.

The third paper, [3], has analyzed the [16-19] turbulence models, applied to the problem of the simplified VLS. The [16] model was one-equation, whereas the others were two-equation models. The [18] model was studied in its four variants, as also the [19] model. In the former, the Wilcox, two-layer, BSL and SST variants were studied. In the latter, the four combinations involving the [20-21] versions were tested. The best

performance was due to the [18] model in the BSL variant. This version has presented the best estimative of the stagnation pressure and the second best estimative of the lift aerodynamic coefficient.

Finally, the fourth paper, [4], has studied the [22-23] models, the later in its [21] and [24] variants, and the [25-27] models. All turbulence models were two-equation models. The best performance was due to the [23] model, in its [24] variant, because has presented the best estimative of the stagnation pressure and the best estimative of the lift aerodynamic coefficient.

With the result of these four papers, the present work consists in the solution of the two-dimensional Favre-averaged Navier-Stokes equations using an upwind discretization on a structured mesh to determine the best turbulence model of this study. The [5] scheme is employed to perform the numerical experiments. The [11], [14], [18], and [23] turbulence models are used in order to close the problem. The [11] model is algebraic, whereas the others are two-equation models. The physical problem under study is the supersonic flow along a ramp configuration. The implemented scheme uses a MUSCL procedure to reach second order accuracy in space. The time integration uses a Runge-Kutta method of five stages and is second order accurate. The algorithm is accelerated to the steady state solution using a spatially variable time step. This technique has proved excellent gains in terms of convergence rate as reported in [6-7] works. The results have demonstrated that the [23] model in its LS variant has yielded consistent wall pressure distribution. The [23] model in its LS variant also captured the boundary layer detachment with consequent detection of circulation bubble formation. Finally, the shock angle is better predicted by the [23] turbulence model in its LS variant.

## 2. Results

Tests were performed in a Dual Core processor of 2.3GHz and 2.0Gbytes of RAM microcomputer. Three orders of reduction of the maximum residual in the field were considered to obtain a converged solution. The residual was defined as the value of the discretized conservation equation. The entrance or attack angle was adopted equal to zero. The ratio of specific heats,  $\gamma$ , assumed the value 1.4. The Reynolds number was estimated based on [28] data.

Figures 1 shows the ramp configuration, whereas Fig. 2 shows the ramp mesh. A mesh of 61x60 points or composed of 3,540 rectangular cells and 3,660 nodes was generated, employing an exponential stretching of 10.0% in the  $\eta$  direction. The initial data of the simulations are described in Tab. 1.

Table 1. Initial Conditions.

$M_\infty$	$\theta$	Altitude	$L_\infty$	Re
2.0	0.0°	20,000m	0.0437m	$1.61 \times 10^5$

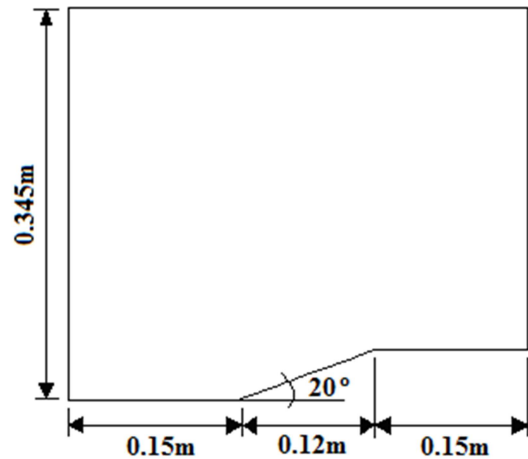


Figure 1. Ramp configuration.

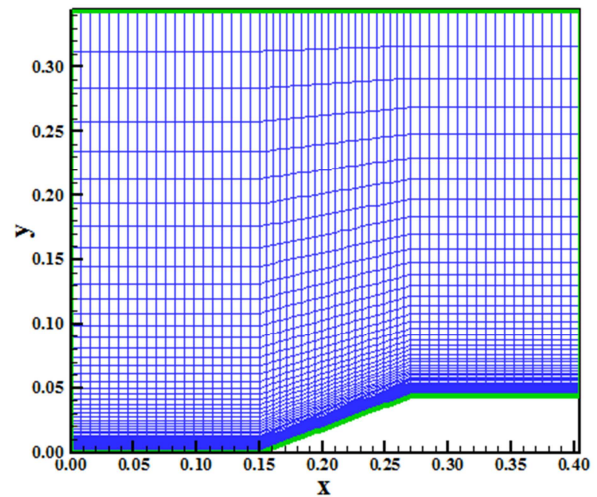


Figure 2. Ramp viscous mesh.

### 2.1. Baldwin and Lomax Results

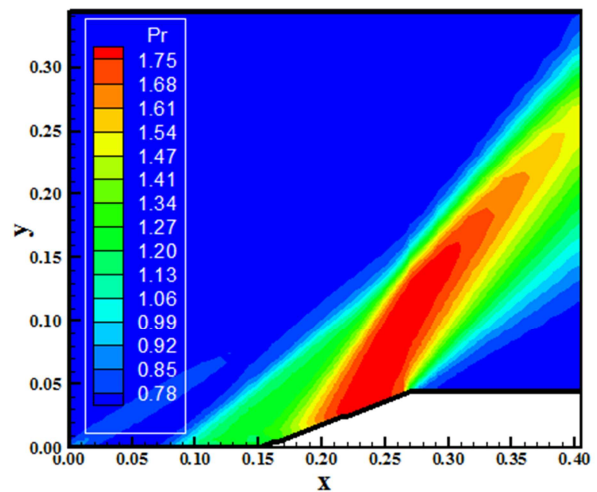


Figure 3. Pressure contours (BL).

Figure 3 exhibit the pressure contours obtained by the

second order [5] scheme as using the [11] turbulence model. The contours are uniform and well defined. The oblique shock wave at the ramp corner is well captured. A weak shock wave is formed upstream the ramp corner. This shock indicates the formation of a circulation bubble close to the ramp corner.

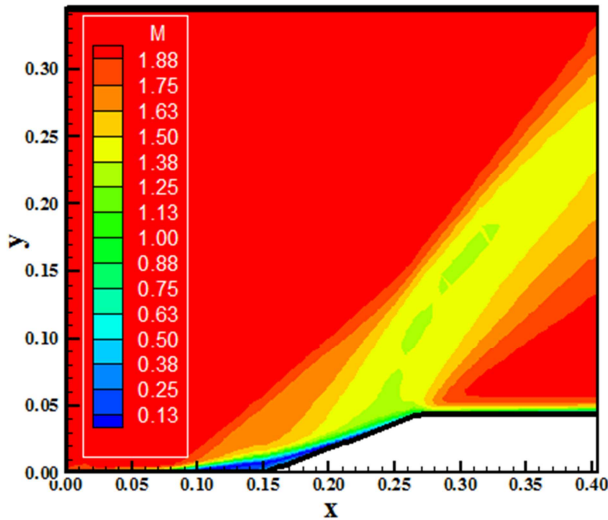


Figure 4. Mach number contours (BL).

This circulation bubble is the result of the boundary layer detachment due to viscous effects at the wall.

Figure 4 exhibits the Mach number contours obtained by the high resolution TVD [5] scheme as using the [11] turbulence model. The viscous region close to the ramp wall is well captured. The boundary layer detachment is verified by the intense energy exchange in the corner region. The formation of a circulation bubble is well characterized in this figure. The solution is free of pre-shock oscillations.

Due to the boundary layer detachment and the formation of a region of intense energy exchange, a circulation bubble is formed close to the ramp corner. This is shown in Figure 5, where the bubble was appropriately captured by the numerical scheme and turbulence model.

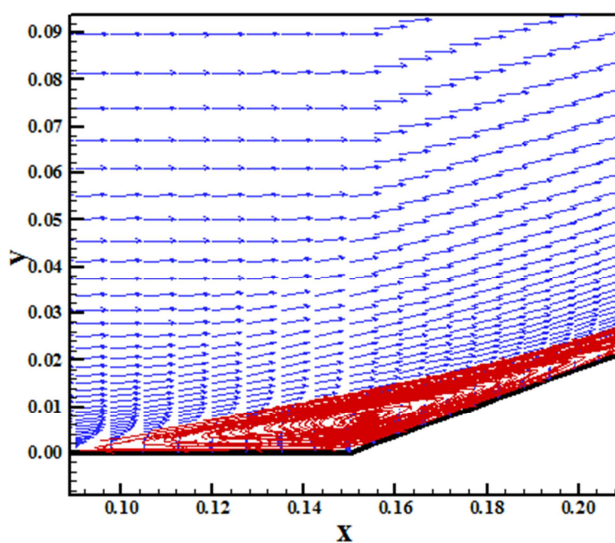


Figure 5. Circulation bubble formation (BL).

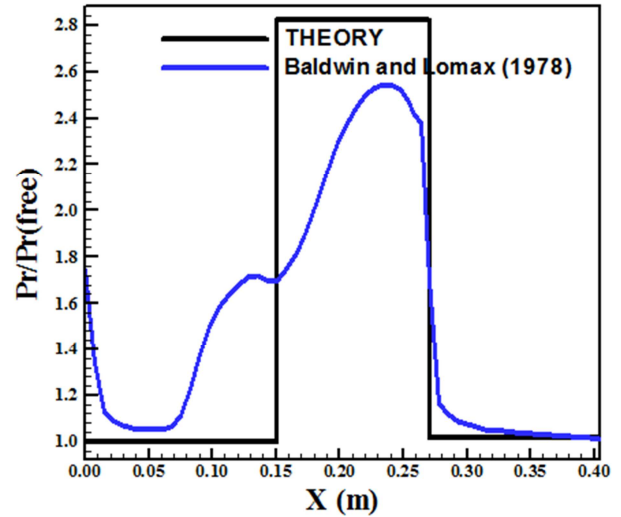


Figure 6. Wall pressure distribution (BL).

Figure 6 shows the pressure distribution along the ramp wall. The theoretical solution is plotted in conjunction because it should be the solution if the viscous effects did not predominate. As can be seen, the numerical pressure plateau is well below the theoretical pressure plateau, due to viscous effects. In all this distribution, no overshoots and undershoots are perceptible, even for a second-order scheme. This aspect highlights the MUSCL procedure as a good tool to provide clean profiles. Such procedure avoids the appearance of Gibbs phenomenon, typical of second order schemes, yielding good quality solutions.

## 2.2. Wilcox Results

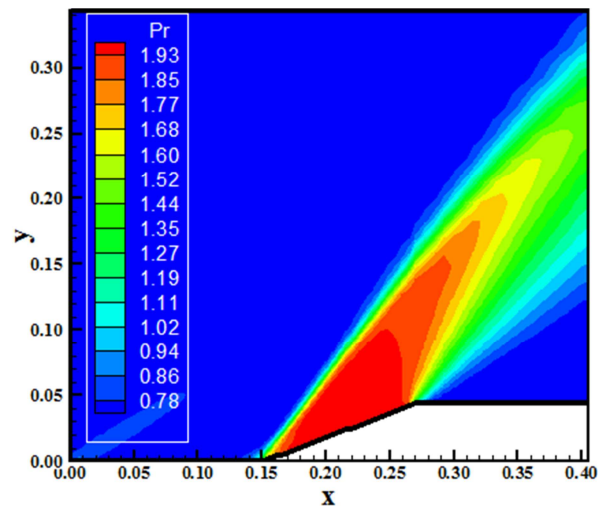


Figure 7. Pressure contours (W).

Figure 7 shows the pressure contours obtained by the [5] scheme as using the [14] turbulence model. The shock is well defined and homogeneous. As can be seen, there are qualitative differences between this plot and the [11] corresponding plot. The oblique shock at the corner region is captured by both models, but the second shock is not captured by the [14] model. The boundary layer detachment is not observed in the [14] solution, which implies that the

circulation bubble is not formed.

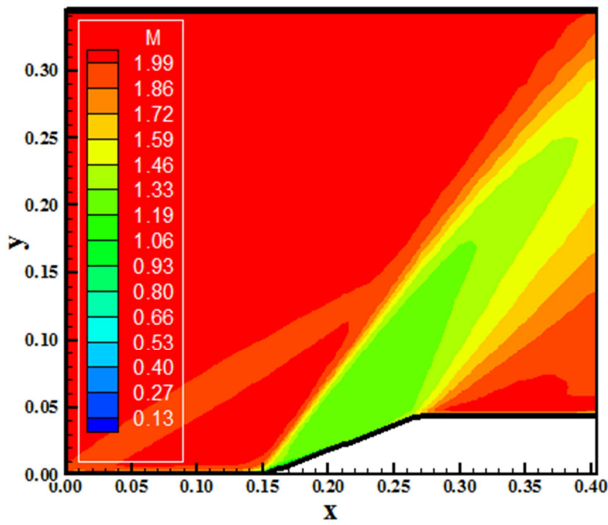


Figure 8. Mach number contours (W).

From the experience in other works [30-35], the appearance of the weak shock wave before the ramp is an undoubtable fact and the turbulence model should be able to capture this non-linearity. The above result indicates that the [14] turbulence model was not able to capture this phenomenon and it penalizes its description of the flow field.

Figure 8 exhibits the Mach number contours obtained by the [5] numerical scheme as using the [14] turbulence model. The present contours are very distinct of the [11] solution. The circulation bubble as a result of the boundary layer detachment is not formed. The shock is well characterized, but the region of intense energy exchange is not highlighted.

No regions of circulation bubbles are captured by the [14] turbulence model. The detail of the corner region shows an attached boundary layer with no circulation bubble formation, which is a severe penalization to this turbulence model. This separation was captured by the studied turbulence models of the [30-35] works, what becomes improbable its inexistence.

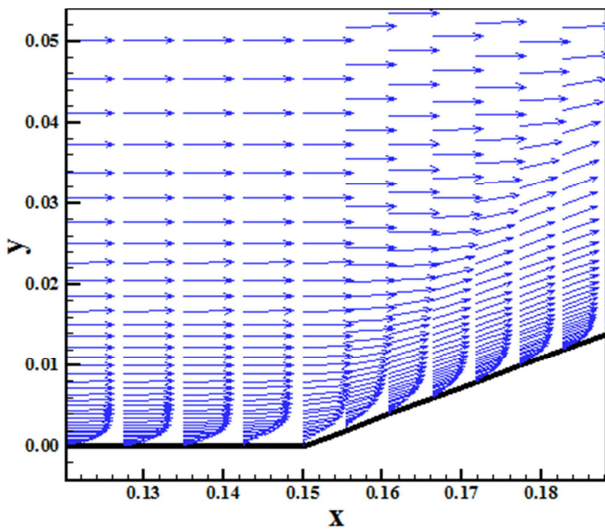


Figure 9. Circulation bubble formation (W).

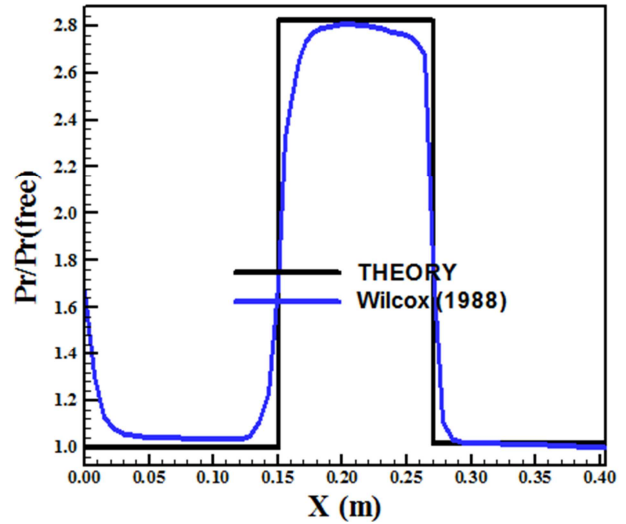


Figure 10. Wall pressure distribution (W).

Figure 10 presents the pressure distribution at wall of the ramp configuration, generated by the [14] turbulence model. This curve is coincident enough to the theoretical results and it would be an excellent solution whether the boundary layer detachment was captured by the turbulence model. The appearance of a small first plateau before the ramp, as occurred in the [11] solution, characterizing the circulation bubble formation, is a typical feature of this type of plot.

### 2.3. Menter and Rumsey BSL Results

Figure 11 shows the pressure contours generated by the [5] scheme as using the [18] turbulence model in its BSL variant. These contours are similar to the contours of the [14] model. The shock is well captured and the solution is not totally homogeneous. It did not present pre-shock oscillations. The first shock, the weak shock, is not captured by this turbulence model and it penalizes its quality solution. As in the [14] solution, the [18] solution did not capture the boundary layer detachment and not circulation bubble was observed.

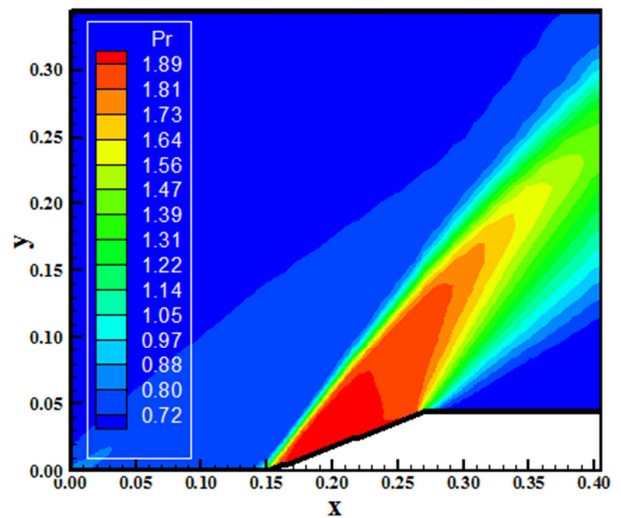


Figure 11. Pressure contours (MR-BSL).

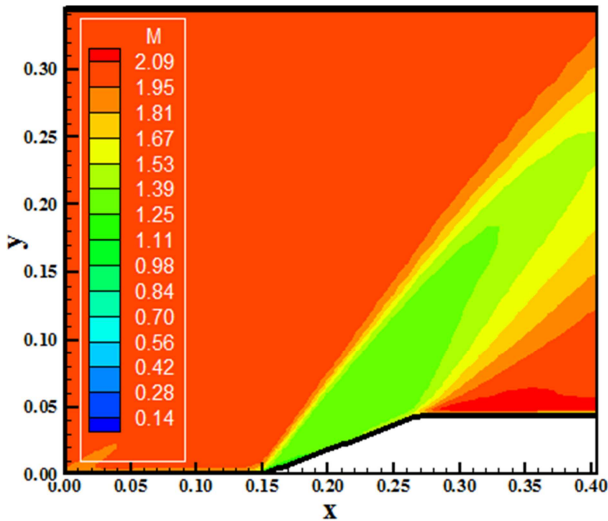


Figure 12. Mach number contours (MR-BSL).

Figure 12 exhibits the Mach number contours obtained as using the [18] turbulence model in its BSL variant. The solution is similar to the [14] solution. It is possible to note that this solution presents less dissipation than the [14] solution. It is clear that the region of intense energy exchange is not formed and this behavior equaled the [14] one.

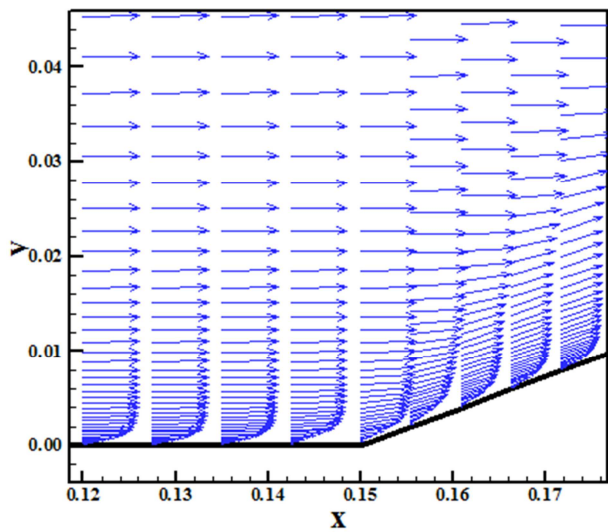


Figure 13. Circulation bubble formation (MR-BSL).

Figure 13 corroborates what was observed in the aforementioned paragraph. Circulation bubbles formation was not observed. Regions of high heating and of generation of loss of energy by the bubbles displacement and energy exchange due to collisions were not observed. This solution agrees with that of the [14] turbulence model.

Figure 14 exhibits the wall pressure distribution resulting from the [18] turbulence model in its BSL variant. The distribution is worse than that of the [11] solution, not capturing the circulation bubble formation as a result of the boundary layer detachment. This solution is closer to the [14] solution, presenting a worse behavior at the fan pressure.

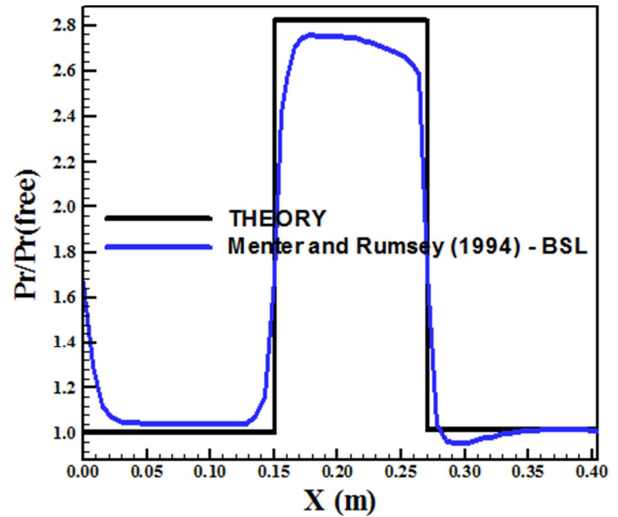


Figure 14. Wall pressure distribution (MR-BSL).

## 2.4. Kergaravat and Knight LS Results

Figure 15 shows the pressure contours obtained by the [5] algorithm as the [23] turbulence model, in its Launder and Spalding variant, is employed. The curves of contours are well defined and the solution quality is similar to the [11] solution. The weak shock formed ahead of the compression corner is captured and a small circulation bubble is formed as resulted from the boundary layer detachment.

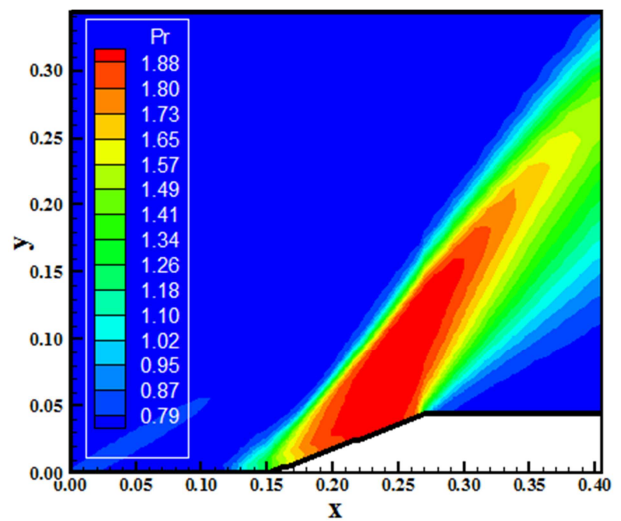


Figure 15. Pressure contours (KK-LS).

Figure 16 exhibits the Mach number contours obtained by the [23] turbulence model as the LS variant is employed. The contours present the same features of the [11] contours, detecting the region of intense energy exchange close to the ramp corner. The circulation bubble formation is clearly captured from the [23] turbulence model in its LS variant. No pre-shock oscillations are perceptible. The primary shock is more homogeneous than the respective shock of the [11] solution.

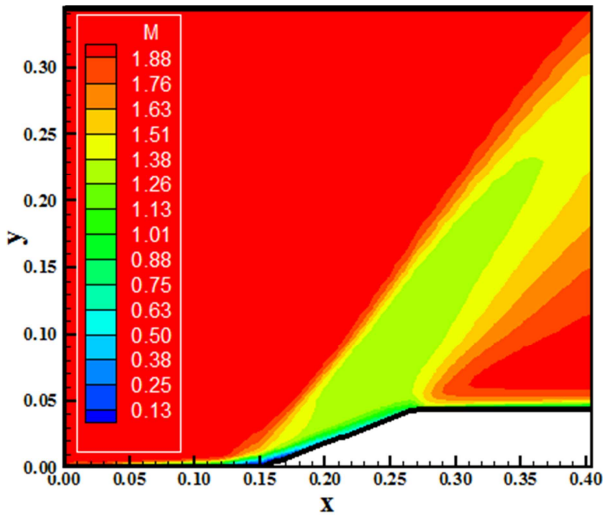


Figure 16. Mach number contours (KK-LS).

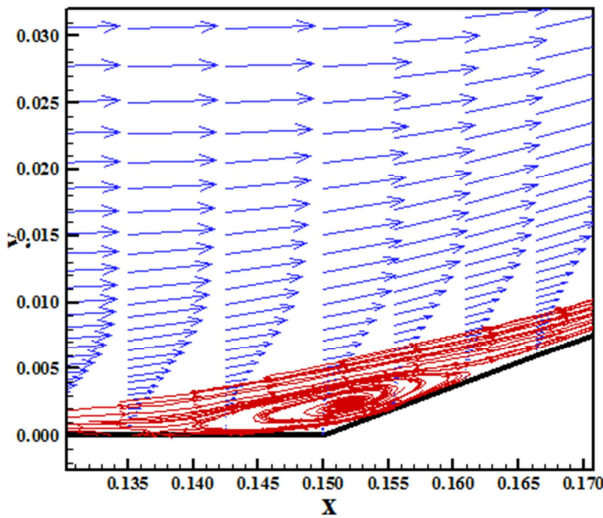


Figure 17. Circulation bubble formation (KK-LS).

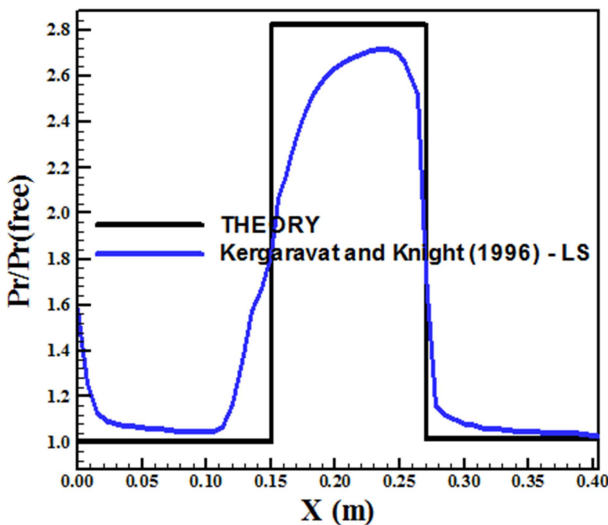


Figure 18. Wall pressure distribution (KK-LS).

Figure 17 shows the circulation bubble formation close to the ramp’s compression corner. The boundary layer

detachment causes the appearance of this phenomenon. A region of intense energy exchange is established. This circulation bubble is smaller than that observed in the [11] solution, but it does not degenerate the pressure profile enough.

Figure 18 shows the wall pressure distribution obtained with the [23] turbulence model in its LS variant. This pressure profile detects the boundary layer detachment and is close to the theoretical pressure profile. In other words, the [23] turbulence model presents a compromise between capture of non-linearity and shock strength features.

### 2.5. Quantitative Analysis

One way to quantitatively verify if the solutions generated by each model are satisfactory consists in determining the shock angle of the oblique shock wave,  $\beta$ , measured in relation to the initial direction of the flow field. [29] (pages 352 and 353) presents a diagram with values of the shock angle,  $\beta$ , to oblique shock waves. The value of this angle is determined as function of the freestream Mach number and of the deflection angle of the flow after the shock wave,  $\phi$ . To  $\phi = 20^\circ$  (ramp inclination angle) and to a freestream Mach number equals to 2.0, it is possible to obtain from this diagram a value to  $\beta$  equals to  $53.0^\circ$ . Using a transfer in Figures 3, 7, 11, and 15 it is possible to obtain the values of  $\beta$  estimated by each turbulence model, as well the respective errors, shown in Tab. 2. It is possible to distinguish that the [5] scheme using the [23] turbulence model, in its LS variant, yields the best result with 0.94% of error. Hence, in terms of accuracy the [23] turbulence model in its LS variant is the best.

Table 2. Values of the stagnation pressure and respective percentage errors.

Turbulence Model:	$\beta$ (°):	Error (%):
[11] turbulence model	51.0	3.77
[14] turbulence model	52.0	1.89
[18] turbulence model	51.0	3.77
[23] turbulence model	53.5	0.94

Finally, Table 3 exhibits the computational data of the present simulations. It can be noted that the most efficient is the [18] turbulence model.

Table 3. Computational data.

Turbulence Model:	CFL:	Iterations:
[11] turbulence model	0.10	32,144
[14] turbulence model	0.10	2,825
[18] turbulence model	0.10	2,095
[23] turbulence model	0.10	6,592

As final conclusion of this study, the [23] turbulence model in its Launder and Spalding variant was the best when comparing these four turbulence models: [11, 14, 18, 23]. This choice is based on the best behavior in the capture of non-linearity like boundary layer detachment with circulation bubble formation and in the estimative of shock angle of the

oblique shock wave. Considering all seventeen turbulence models studied in these five papers, the [23] turbulence model in its Launder and Spalding variant is the best.

### 3. Conclusions

The present work consists in the solution of the two-dimensional Favre-averaged Navier-Stokes equations using an upwind discretization on a structured mesh. The [5] scheme is employed to perform the numerical experiments. The [11], [14], [18], and [23] turbulence models are used in order to close the problem. The [11] model is algebraic, whereas the others are two-equation models. The physical problem under study is the supersonic flow along a ramp configuration. The implemented scheme uses a MUSCL procedure to reach second order accuracy in space. The time integration uses a Runge-Kutta method of five stages and is second order accurate. The algorithm is accelerated to the steady state solution using a spatially variable time step. This technique has proved excellent gains in terms of convergence rate as reported in [6-7] works. The results have demonstrated that the [23] model in its LS variant has yielded consistent wall pressure distribution. The [23] model in its LS variant also captured the boundary layer detachment with consequent detection of circulation bubble formation. Finally, the shock angle is better predicted by the LS [23] turbulence model.

This paper finishes our work related to the study of seventeen turbulence models applied to the solution of aerospace problems in the supersonic flow regime. It was applied the [5] TVD scheme to perform the numerical experiments. The supersonic flows around a simplified VLS configuration and along a ramp were studied. The best quantitative results were obtained with the [23] turbulence model in its Launder and Spalding variant, highlighting this one as the best of all.

### Acknowledgment

The author would like to thank the infrastructure of ITA that allowed the realization of this work.

### References

- [1] E. S. G. Maciel, "Assessment of Several Turbulence Models as Applied to Supersonic Flows in 2D – Part I", Submitted to Engineering and Technology (under review), 2015.
- [2] E. S. G. Maciel, "Assessment of Several Turbulence Models as Applied to Supersonic Flows in 2D – Part II", Submitted to Engineering and Technology (under review), 2015.
- [3] E. S. G. Maciel, "Assessment of Several Turbulence Models as Applied to Supersonic Flows in 2D – Part III", Submitted to Engineering and Technology (under review), 2015.
- [4] E. S. G. Maciel, "Assessment of Several Turbulence Models as Applied to Supersonic Flows in 2D – Part IV", Submitted to Engineering and Technology (under review), 2015.
- [5] B. Van Leer, "Flux-Vector Splitting for the Euler Equations", Proceedings of the 8th International Conference on Numerical Methods in Fluid Dynamics, E. Krause, Editor, Lecture Notes in Physics, vol. 170, pp. 507-512, Springer-Verlag, Berlin, 1982.
- [6] E. S. G. Maciel, "Analysis of Convergence Acceleration Techniques Used in Unstructured Algorithms in the Solution of Aeronautical Problems – Part I", Proceedings of the XVIII International Congress of Mechanical Engineering (XVIII COBEM), Ouro Preto, MG, Brazil, 2005. [CD-ROM]
- [7] E. S. G. Maciel, "Analysis of Convergence Acceleration Techniques Used in Unstructured Algorithms in the Solution of Aerospace Problems – Part II", Proceedings of the XII Brazilian Congress of Thermal Engineering and Sciences (XII ENCIT), Belo Horizonte, MG, Brazil, 2008. [CD-ROM]
- [8] T. Cebeci, and A. M. O. Smith, "A Finite-Difference Method for Calculating Compressible Laminar and Turbulent Boundary Layers", Journal of Basic Engineering, Trans. ASME, Series B, vol. 92, no. 3, pp. 523-535, 1970.
- [9] W. P. Jones, and B. E. Launder, "The Prediction of Laminarization with a Two-Equation Model of Turbulence", International Journal of Heat and Mass Transfer, vol. 15, pp. 301-304, 1972.
- [10] B. E. Launder, and B. I. Sharma, "Application of the Energy Dissipation Model of Turbulence to the Calculation of Flow Near a Spinning Disc", Letters in Heat and Mass Transfer, vol. 1, no. 2, pp. 131-138, 1974.
- [11] B. S. Baldwin, and H. Lomax, "Thin Layer Approximation and Algebraic Model for Separated Turbulent Flows", AIAA Paper 78-257, 1978.
- [12] D. C. Wilcox, and M. W. Rubesin, "Progress in Turbulence Modeling for Complex Flow Fields Including the Effects of Compressibility", NASA TP-1517, 1980.
- [13] T. J. Coakley, "Turbulence Modeling Methods for the Compressible Navier-Stokes Equations", AIAA Paper No. 83-1693, 1983.
- [14] D. C. Wilcox, "Reassessment of the Scale-Determining Equation for Advanced Turbulence Models", AIAA Journal, Vol. 26, November, pp. 1299-1310, 1988.
- [15] P. S. Granville, "Baldwin Lomax Factors for Turbulent Boundary Layers in Pressure Gradients", AIAA Journal, Vol. 25, pp. 1624-1627, 1989.
- [16] P. R. Spalart, and S. R. Allmaras, "A One-Equation Turbulence Model for Aerodynamic Flows", AIAA Paper 92-0439, 1992.
- [17] F. Jacon, and D. Knight, "A Navier-Stokes Algorithm for Turbulent Flows Using an Unstructured Grid and Flux Difference Splitting", AIAA Paper 94-2292, 1994.
- [18] F. R. Menter, and C. L. Rumsey, "Assessment of Two-Equation Turbulence Models for Transonic Flows", AIAA Paper 94-2343, 1994.
- [19] M. M. Gibson, and A. A. Dafa'Alla, "Two-Equation Model for Turbulent Wall Flow", AIAA Journal, Vol. 33, No. 8, pp. 1514-1518, 1995.
- [20] B. E. Launder, and B. I. Sharma, Application of the Energy-Dissipation Model of Turbulence to the Calculation of Flow Near a Spinning Disc, Letters in Heat and Mass Transfer, Vol. 1, No. 2, pp. 131-138, 1974.

- [21] K. Y. Chien, "Predictions of Channel and Boundary Layer Flows with a Low-Reynolds-Number Turbulence Model", *AIAA Journal*, Vol. 20, January, pp. 33-38, 1982.
- [22] G. Zhou, L. Davidson, and E. Olsson, "Turbulent Transonic Airfoil Flow Simulation Using a Pressure-Based Algorithm", *AIAA Journal*, Vol. 33, No. 1, January, pp. 42-47, 1995.
- [23] Y. Kergaravat, and D. Knight, "A Fully Implicit Navier-Stokes Algorithm for Unstructured Grids Incorporating a Two-Equation Turbulence Model", *AIAA Paper 96-0414*, 1996.
- [24] B. E. Launder, and D. B. Spalding, "The Numerical Computation of Turbulent Flows", *Computer Methods in Applied Mechanics and Engineering*, vol. 3, pp. 269-289, 1974.
- [25] D. A. Yoder, N. J. Georgiadids, and P. D. Orkwis, "Implementation of a Two-Equation K-Omega Turbulence Model in NPARC", *AIAA Paper 96-0383*, 1996.
- [26] T. J. Coakley, "Development of Turbulence Models for Aerodynamic Applications", *AIAA Paper 97-2009*, 1997.
- [27] C. L. Rumsey, T. B. Gatski, S. X. Ying, and A. Bertelrud, "Prediction of High-Lift Flows Using Turbulent Closure Models", *AIAA Journal*, Vol. 36, No. 5, May, pp. 765-774, 1998.
- [28] R. W. Fox, and A. T. McDonald, "Introdução à Mecânica dos Fluidos", Ed. Guanabara Koogan, Rio de Janeiro, RJ, Brazil, 632 p, 1988.
- [29] J. D. Anderson Jr., "Fundamentals of Aerodynamics", McGraw-Hill, Inc., EUA, 563p, 1984.
- [30] E. S. G. Maciel, "Aplicações de Algoritmos Predictor-Corretor e TVD na Solução das Equações de Euler e de Navier-Stokes em Duas Dimensões", Ed. Universidade Federal de Pernambuco, 315p., 2013.
- [31] E. S. G. Maciel, "Aplicações de Algoritmos TVD na Solução das Equações de Euler e de Navier-Stokes em Duas Dimensões", Ed. Universidade Federal de Pernambuco, 169p., 2013.
- [32] E. S. G. Maciel, "Aplicações de Algoritmos Simétricos, TVD e ENO na Solução das Equações de Euler e de Navier-Stokes em Duas Dimensões", Ed. Universidade Federal de Pernambuco, 229p., 2014.
- [33] E. S. G. Maciel, "Laminar and Turbulent Simulations of Several TVD Schemes in Two-Dimensions - Part I - Results", *Computational Problems in Engineering*, Springer-Verlag, pp. 203-229, 2014.
- [34] E. S. G. Maciel, and O. Seye, "Laminar and Turbulent Simulations of Several TVD Schemes in Two-Dimensions – Theory", *Proceedings of the XIII Jornadas de Mecânica Computacional (XIII JMC)*, Curicó, Chile, vol. 12, pp. 177-185, 2014.
- [35] E. S. G. Maciel, and O. Seye, "Laminar and Turbulent Simulations of Several TVD Schemes in Two-Dimensions – Results", *Proceedings of the XIII Jornadas de Mecânica Computacional (XIII JMC)*, Curicó, Chile, vol. 12, pp. 186-194, 2014.